

DiffPatch: Generating Customizable Adversarial Patches using Diffusion Model

Zhixiang Wang¹, Guangnan Ye¹, Xiaosen Wang², Siheng Chen³, Zhibo Wang⁴,
Xingjun Ma^{1*}, Yu-Gang Jiang¹

¹Shanghai Key Lab of Intell. Info. Processing, School of CS, Fudan University
²Huawei Technologies Ltd. ³Shanghai Jiao Tong University ⁴Zhejiang University

Abstract

Physical adversarial patches printed on clothing can easily allow individuals to evade person detectors. However, most existing adversarial patch generation methods prioritize attack effectiveness over stealthiness, resulting in patches that are aesthetically displeasing. Although existing methods using generative adversarial networks or diffusion models can produce more natural-looking patches, they often struggle to balance stealthiness with attack effectiveness and lack flexibility for user customization. To address these challenges, we propose a novel diffusion-based customizable patch generation framework termed **DiffPatch**, specifically tailored for creating naturalistic and customizable adversarial patches. Our approach enables users to utilize a reference image as the source, rather than starting from random noise, and incorporates masks to craft naturalistic patches of various shapes, not limited to squares. To prevent the original semantics from being lost during the diffusion process, we employ Null-text inversion to map random noise samples to a single input image and generate patches through Incomplete Diffusion Optimization (IDO). Notably, while maintaining a natural appearance, our method achieves a comparable attack performance to state-of-the-art non-naturalistic patches when using similarly sized attacks. Using DiffPatch, we have created a physical adversarial T-shirt dataset, **AdvPatch-1K**, specifically targeting YOLOv5s. This dataset includes over a thousand images across diverse scenarios, validating the effectiveness of our attack in real-world environments. Moreover, it provides a valuable resource for future research.

1. Introduction

With the rapid advancement of computer vision, object detectors are extensively utilized in real-world scenarios, including fields such as autonomous driving [8] and medical diagnostics [33]. Unfortunately, recent works [7, 15, 45, 47]

*Corresponding author: xingjunma@fudan.edu.cn



Figure 1. Example images from our **AdvPatch-1K** dataset, showcasing the performance of DiffPatch in various scenarios.

have demonstrated that deep neural networks are vulnerable to maliciously crafted adversarial examples, resulting in decisions that defy common sense. This poses significant threats to safety-critical applications.

In the field of computer vision, adversarial attacks can be categorized into two distinct groups: digital attacks [7, 17] and physical attacks [14, 27, 32]. Different from digital attacks, which involve introducing small perturbations within a digital domain, physical adversarial attacks operate in the tangible world, aiming to mislead visual systems through modifications to the appearance or positioning of physical objects. The execution of physical adversarial attacks can be accomplished through numerous methods, including the application of adversarial patches onto the surface of an object, alterations in environmental lighting conditions, or the introduction of distracting elements.

For physical-world adversarial patches, previous research [43, 48] has primarily focused on enhancing attack performance, which often requires introducing stronger perturbations that significantly deviate patches from the distribution of natural images, making them appear highly unnatural. While most patch generation methods [23, 46] incorporate a total variation loss to smooth the patches, this fun-

damental issue remains unresolved, rendering the patches easily identifiable by humans. With the rapid development of image generation techniques [16, 20], naturalistic patch generation methods based on deep image generators have gradually emerged [21, 30]. The patches generated by state-of-the-art generators possess a more natural appearance, significantly enhancing their stealthiness. However, these methods suffer from limited attack effectiveness compared to unnatural patches. Moreover, these methods have high randomness in the generation process, making it difficult to generate customized patches based on a given image.

In this work, we propose a novel Stable Diffusion [39] based adversarial patch generation method called **DiffPatch** that is capable of generating a naturalistic and customizable adversarial patch based on a reference image specified by the adversary. Our DiffPatch method works as follows. Firstly, it maps the reference image into the latent space and generates adversarial patches by optimizing the noise latent vectors. It adopts Null-text inversion [34] to achieve a near-perfect reconstruction so as to guarantee that the generated images largely preserve the original semantics. Secondly, it introduces an *Incomplete Diffusion Optimization (IDO)* strategy to ensure the natural appearance and attack performance of the optimized patches and employs an IoU-Detection loss to accelerate convergence. Furthermore, to generate irregular-shaped patches, it utilizes masks to replace the background and covers the gradients in non-essential areas. This can also help reduce information interference from other regions during the optimization process. Based on DiffPatch, we have created an adversarial patch dataset **AdvPatch-1K** which consists of over a thousand images, featuring attacks in various physical-world scenarios with customizable patches of diverse styles and shapes. Partial results are shown in Figure 1. Our main contributions are as follows:

- We propose a novel diffusion-based method called **DiffPatch** for generating naturalistic adversarial patches based on a reference image. DiffPatch employs Null-text inversion, *Incomplete Diffusion Optimization (IDO)*, masked customization, and an IoU-Detection loss to generate stylized and customizable adversarial patches.
- Experimental results show that our DiffPatch achieves the highest attack success rate (ASR), significantly reducing the mAP of various object detectors, rivaling or even surpassing the current state-of-the-art methods of unnatural adversarial patches.
- We create physical-world adversarial patches by printing them on T-shirts and collect a dataset, **AdvPatch-1K**, which consists of 1,131 images with annotations. This dataset covers 9 unique adversarial T-shirt designs across various contexts, including both indoor and outdoor settings as well as individual and group photos.

2. Related Work

2.1. Physical Adversarial Attack

With the widespread application of deep learning, researchers began to investigate the security of these models in real-world scenarios. This focus led to the development of the Basic Iterative Method (BIM) [27], which generates adversarial samples that retain their adversarial properties even after being printed. To improve the robustness of physical adversarial samples, the Expectation Over Transformation (EOT) approach [2] was introduced. EOT enhances resistance to real-world transformations by simulating various modifications that images may undergo. The Digital-to-Physical (D2P) method [24] further advances real-world attack effectiveness by learning the transformations between digital and physical images. AdvPatch [5] marks a milestone by demonstrating the creation of robust adversarial patches that function reliably across diverse environmental conditions. Following this, AdvYOLO [43] demonstrated an attack on object detectors by applying adversarial patches to clothing surfaces, allowing wearers to evade detection. Several similar patch attack methods have since been proposed [22, 46, 48, 52], posing a significant threat to object detectors. Additionally, other physical adversarial attack methods have employed accessories like glasses [41], lighting [51], and shadows [50].

2.2. Naturalistic Adversarial Patch

Inspired by the imperceptibility constraints in digital attacks, Universal Physical Camouflage Attacks (UPC) [23] employ the L_∞ norm to limit perturbations and maintain the natural appearance of patches. Unlike iterative methods that optimize patches on images, the Naturalistic Adversarial Patch (NAP) [21] utilizes a generative approach. NAP leverages GANs to indirectly optimize the patch by modifying initial latent vectors, resulting in patches with a highly natural appearance. Building on these advancements, several GAN-based generation methods have emerged [13, 28]. Additionally, diffusion model-based methods have gained traction in the vision field [9, 30, 49]. The generative power of diffusion models enables the creation of more naturalistic and effective physical adversarial patches.

2.3. Diffusion-based Image Editing

Recently, diffusion models have excelled in the field of image generation, with models like DALL-E2 [36], Imagen [40], and Stable Diffusion [39] largely surpassing GANs in performance [12]. Beyond generation tasks, diffusion-based image editing techniques have also become mainstream. Leveraging the cross-attention mechanism, Prompt to Prompt (P2P) [18] introduces an innovative framework that enables image editing solely through text prompts. To address challenges with poor reconstruction during editing,

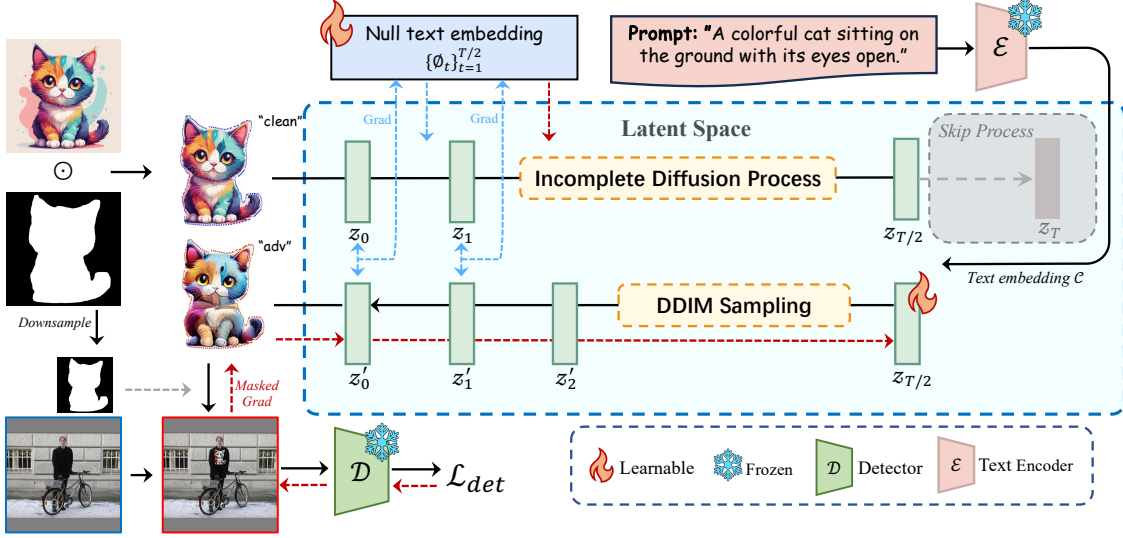


Figure 2. An overview of the proposed *DiffPatch* generation framework.

Null-text inversion [34] achieves near-perfect reconstruction by optimizing the unconditional embedding at each denoising step. Text-driven Blended Diffusion [3] employs masks to target specific regions in an image, allowing for background replacement and consistent edits within defined areas. Additionally, some adversarial attack methods [10, 49] leverage image editing techniques to modify images while preserving their natural appearance, creating adversarial examples that are visually coherent yet misleading to detection models.

3. Proposed Approach

Overview Figure 2 provides an overview of *DiffPatch*. It optimizes the Null text embeddings along incomplete diffusion trajectories and maps the image to the latent vectors at intermediate timestamps, ensuring that the patch maintains a natural appearance during updates. It then applies the Incomplete Diffusion Optimization (IDO) guided by an IoU-Detection Loss to optimize the latent vectors, resulting in faster convergence and enhanced attack performance. During optimization, we skip the U-Net gradients to avoid memory overflow and utilize target masks to eliminate semantic interference from irrelevant areas, thereby generating more naturalistic adversarial patches. Next, we will introduce the key techniques used in *DiffPatch*.

3.1. Image-to-Latent Mapping

Our objective is to achieve a perfect mapping between a given image \mathcal{I} and latent vector z_t , utilizing the image encoding z_0 to obtain z_t , which is essentially the reverse process of DDIM sampling [42]. Based on the assumption that the ODE process can be reversed in the limit of small steps,

DDIM inversion can be formulated as:

$$z_{t+1} = \sqrt{\frac{\alpha_{t+1}}{\alpha_t}} z_t + \left(\sqrt{\frac{1}{\alpha_{t+1}} - 1} - \sqrt{\frac{1}{\alpha_t} - 1} \right) \cdot \varepsilon_\theta(z_t, t, \mathcal{C}), \quad (1)$$

where ε_θ is the pre-trained U-Net used to predict noise, \mathcal{C} is the condition embedding of \mathcal{P} , and α_t is calculated based on the schedule $\beta_0, \dots, \beta_T \in (0, 1)$, i.e., $\alpha_t = \prod_{i=1}^t (1 - \beta_i)$. Through the aforementioned formula, we can obtain the latent vector z_t and utilize it for image reconstruction, yet this does not guarantee perfect reconstruction.

To enhance the quality of generated outputs, Stable Diffusion incorporates a classifier-free guidance mechanism [19] that concurrently engages in unconditional generation and guided generation based on condition embedding \mathcal{C} :

$$\tilde{\varepsilon}_\theta(z_t, t, \mathcal{C}, \phi) = w \cdot \varepsilon_\theta(z_t, t, \mathcal{C}) + (1 - w) \cdot \varepsilon_\theta(z_t, t, \phi), \quad (2)$$

where w represents the guidance scale parameter, and $\phi = \mathcal{E}(\text{" "})$ is the embedding of a null text. The generated content is highly sensitive to textual prompts. During each step of guided generation, even minor variations in the prompt can lead to deviations in the trajectory. This cumulative error can make reconstruction challenging, and such errors tend to amplify when we perform image editing.

To resolve this issue, we separately optimize the null text embedding ϕ_t for each timestamp t in the order of the diffusion process $t = T \rightarrow t = 1$, using the optimized embedding to guide the process back onto the correct trajectory. Similar to Null-text inversion [34], firstly, we set the guidance scale w to 1 and utilize DDIM inversion to obtain intermediate vectors z_T^*, \dots, z_0^* where $z_0^* = z_0$. After that, regarding z_T^* as the initial noise vector \bar{z}_T , we optimize the null text embedding ϕ_t through the application of

the following objective function, after each iteration of the DDIM sampling step (adopting the default value of 7.5 for the guidance scale w):

$$\min_{\phi_t} \|z_{t-1}^* - z_{t-1}(\bar{z}_t, \phi_t, \mathcal{C})\|_2^2, \quad (3)$$

where z_{t-1} represents the vector obtained after DDIM sampling, and after each step of optimization is completed, we update $\bar{z}_{t-1} = z_{t-1}$. Finally, we can achieve near-perfect reconstruction by utilizing the initial noise vector \bar{z}_T and the optimized unconditional embeddings $\{\phi_t\}_{t=1}^T$.

3.2. Incomplete Diffusion Optimization

We propose Incomplete Diffusion Optimization (IDO), which adds adversarial perturbations along the trajectory of image reconstruction. IDO consists of two techniques: 1) IoU-Detection Loss and 2) Incomplete Diffusion Process.

IoU-Detection Loss Loss function is crucial in guiding the optimization process. After an intermediate adversarial image is fed into the detector, we obtain the following outputs: 1) B_{box} : coordinates of the predicted bounding box; 2) P_{obj} : probability indicating the presence of an object within the predicted box; and 3) P_{cls} : classification probabilities for various objects. Previous work used Common Detection Loss [43] to guide adversarial patch generation:

$$\mathcal{L}_{det} = \frac{1}{N} \sum_{i=1}^N \max_j (P_{obj}^j(I_i') \cdot P_{cls}^j(I_i')), \quad (4)$$

where N represents the batch size, and I_i' refers to the i -th image in a batch. For each image I_i' , the detector identifies multiple objects and assigns an index j to each detected object. The images $\{I_i'\}_{i=1}^N$ are obtained by performing operation \mathcal{T} on clean images, which means pasting patches on the surface of the clothes of the person inside.

According to the loss function formulation in Equation (4), the optimization for a given image I_i' is guided solely by the object with the highest confidence product, aiming to minimize the detection probability for that specific target. However, this strategy introduces several challenges. First, the application of adversarial patches is constrained by the availability and accuracy of dataset labels. Incomplete annotations or misdetections can result in critical surfaces remaining unpatched, undermining the optimization process. Moreover, focusing the loss on a single object per iteration leads to slower convergence and increased instability during training, limiting the overall effectiveness of the approach.

We propose an alternative loss function **IoU-Detection Loss** to address these issues. Formally, it is defined as:

$$\mathcal{L}_{IoU} = \frac{1}{N} \sum_{i=1}^N \left(\frac{1}{M} \sum_{k=1}^K \left[\mathbb{1} \left(\max_j \text{IoU}(J_j, J'_k) > t \right) P(J'_k) \right] \right), \quad (5)$$

where M is the total number of detected bounding boxes with an Intersection over Union (IoU) greater than a threshold t with any ground truth box, $\text{IoU}(J_j, J'_k)$ represents the IoU between the predicted bounding box J'_k and the ground truth box J_j , $\mathbb{1}(\cdot)$ is an indicator function that equals 1 if the condition inside the parentheses is met and 0 otherwise, and P denotes the product of the object probability P_{obj} and the classification probability P_{cls} . The IoU-Detection Loss accounts for multiple objects with patches applied to a single image and mitigates the impact of non-patched objects on the training process.

Incomplete Diffusion Process We found that using the default 50-step sampling to generate patches often leads to a loss of semantic meaning and natural appearance during optimization. Excessive sampling steps can amplify subtle changes in z_T , causing the image reconstruction trajectory to deviate. During the image-to-latent mapping phase, we can match it with the latent vector $z_{\frac{T}{2}}$ at an intermediate timestamp to mitigate semantic loss. The generation of adversarial patch z_p can then be represented as:

$$z_p = G(\bar{z}_{\frac{T}{2}}, \frac{T}{2}, \mathcal{C}, \{\phi_t\}_{t=1}^{\frac{T}{2}}), \quad (6)$$

where G represents the diffusion model. Generating patches using $z_{\frac{T}{2}}$ shortens the generation path, thereby enhancing the stability of the patches under adversarial guidance. However, as $z_{\frac{T}{2}}$ continues to be updated, it becomes more chaotic, making complete denoising challenging in the later stages of the process. To prevent adversarial perturbations from being noticeable, perturbation values are constrained by an infinity norm in digital attacks. Similarly, we constrain the perturbations δ applied to the latent vector $z_{\frac{T}{2}}$:

$$\delta_t = \text{Proj}_{\infty}(\delta_{t-1} + \Delta\delta, 0, \epsilon), \quad (7)$$

where the perturbation δ is constrained within a sphere centered at 0 with a radius of ϵ through the projection function. This ensures that the internal semantics of $z_{\frac{T}{2}}$ are not excessively lost, enabling the generation of patches with natural appearances through the denoising process.

Specifically, during denoising, 25 steps of DDIM sampling are required, where U-Net performs 25 noise predictions. The denoising process involves removing noise at timestamp t using a sampling recurrence formula to obtain the vector z_{t-1} , then gradually obtaining z_0 , and finally using an image decoder Ψ to restore the image. When optimizing the vector $z_{T/2}$ with the loss function \mathcal{L} , it can be expanded using the chain rule as follows:

$$\nabla_{z_{T/2}} \mathcal{L} = \frac{\partial \mathcal{L}}{\partial x} \cdot \frac{\partial x}{\partial z_p} \cdot \frac{\partial z_p}{\partial z_0} \cdot \frac{\partial z_0}{\partial z_1} \cdot \dots \cdot \frac{\partial z_{T/2-1}}{\partial z_{T/2}}, \quad (8)$$

where z_p represents the adversarial patch obtained through the image encoder Ψ , i.e., $z_p = \Psi(z_0)$, and x is the training

data with z_p attached. For each step of DDIM sampling, it can be expressed as:

$$\frac{\partial z_{t-1}}{\partial z_t} = \sqrt{\frac{\alpha_{t-1}}{\alpha_t}} + \left(\sqrt{\frac{1}{\alpha_{t-1}} - 1} - \sqrt{\frac{1}{\alpha_t} - 1} \right) \cdot \frac{\partial \varepsilon_\theta(z_t, t, \mathcal{C})}{\partial z_t}. \quad (9)$$

Each denoising step requires computing and storing the U-Net gradient, which can lead to memory overflow. However, since the predicted noise $\varepsilon_\theta(z_t, t, \mathcal{C})$ follows a standard normal distribution $\mathcal{N}(0, I)$, we can use the reparameterization trick [10] to bypass the gradient computation of the U-Net and obtain an approximate gradient:

$$\nabla_{z_{T/2}} \mathcal{L} \approx \frac{\partial \mathcal{L}}{\partial x} \cdot \frac{\partial x}{\partial z_p} \cdot \frac{\partial z_p}{\partial z_0} \cdot \sqrt{\frac{1}{\alpha_1}} \cdots \sqrt{\frac{\alpha_{T/2-1}}{\alpha_{T/2}}}. \quad (10)$$

3.3. Target Mask Control

Our method can generate adversarial patches of various shapes, with the process being controlled by the target mask m . Using target masks serves not only to extract patches of different shapes but also plays a crucial role in the natural appearance of the patch. Since Stable Diffusion [39] generates square images, there is environmental information surrounding our target. After selecting the initial image \mathcal{I} , to prevent the background from interfering with the main subject during the optimization process, we need to replace the background with a solid-colored image s before the Image-to-Latent Mapping stage:

$$\mathcal{I}' = \mathcal{I} \odot m + s \odot (1 - m), \quad (11)$$

Additionally, to ensure that the background remains unchanged throughout the update process, we downsample the mask m by a factor of 8 to match the size of latent vectors and overlay gradients outside the target area.

Overall, the DiffPatch generation process starts with Image-to-Latent Mapping. Incomplete Diffusion Optimization is then applied to reduce memory consumption and enhance performance. Finally, Target Mask Control is used to maintain a natural appearance. The generation process is illustrated in Algorithm 1. In addition, the patch can be iteratively optimized using DiffPatch to achieve an accumulative effect, as shown in Figure 3. Specifically, the generated patch can be used to generate a new patch, enabling stronger attack performance while maintaining natural appearance.

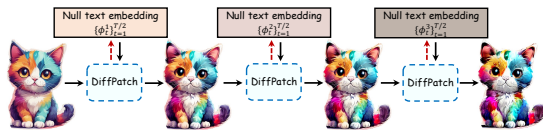


Figure 3. The effect of iterative generation (accumulated style variation from left to right).

Algorithm 1 DiffPatch Generation Process

Input: A patch image \mathcal{I}' with target mask m , prompt embedding $\mathcal{C} = \mathcal{E}(\mathcal{P})$, an object detector \mathcal{D} , training dataset S and ground truth box y .

Parameter: DDIM steps T , unconditional embeddings iteration number N_u , training batch B_t , and patch scale τ .

Output: Adversarial patch

- 1: Compute $z_{\frac{T}{2}}^*, \dots, z_0^*$ using DDIM inversion over \mathcal{I}' with guidance scale $w = 1$
 - 2: Set $w = 7.5$, $\bar{z}_{\frac{T}{2}} \leftarrow z_{\frac{T}{2}}^*$, $\phi_{\frac{T}{2}} \leftarrow \mathcal{E}(\text{" "})$, $\delta_0 \leftarrow 0$
 - 3: **for** $t = \frac{T}{2}, \frac{T}{2} - 1, \dots, 1$ **do**
 - 4: **for** $j = 0, \dots, N_u - 1$ **do**
 - 5: $\phi_t \leftarrow \phi_t - \eta_u \nabla_{\phi} \|z_{t-1}^* - z_{t-1}(\bar{z}_t, \phi_t, \mathcal{C})\|_2^2$
 - 6: **end for**
 - 7: $\bar{z}_{t-1} \leftarrow z_{t-1}(\bar{z}_t, \phi_t, \mathcal{C})$, $\phi_{t-1} \leftarrow \phi_t$
 - 8: **end for**
 - 9: $m^* \leftarrow \text{Downsample}(m)$
 - 10: **for** $k = 1, \dots, N_{iter}$ **do**
 - 11: **for** $b = 1, \dots, B_t$ **do**
 - 12: $X \leftarrow$ Extract the b -th batch of data from S
 - 13: $z_p \leftarrow G(\bar{z}_{\frac{T}{2}} + \delta_{b-1}, \frac{T}{2}, \mathcal{C}, \{\phi_t\}_{t=\frac{T}{2}}) \odot m$
 - 14: $X' \leftarrow \mathcal{T}(z_p, X, \tau)$
 - 15: $g_b \leftarrow \text{Adam}(\nabla_{\bar{z}_{\frac{T}{2}}} \mathcal{L}_{IoU}(\mathcal{D}(X'), y))$
 - 16: $\delta_b \leftarrow \text{Proj}_{\infty}(\delta_{b-1} + \eta_p \cdot g_b, 0, \epsilon) \odot m^*$
 - 17: **end for**
 - 18: Set $\delta_0 = \delta_B$
 - 19: **end for**
 - 20: $z_p \leftarrow G(\bar{z}_{\frac{T}{2}} + \delta_B, \frac{T}{2}, \mathcal{C}, \{\phi_t\}_{t=\frac{T}{2}}) \odot m$
 - 21: **return** z_p
-

4. Experiments

4.1. Experimental Setup

Datasets In our experiments, we trained and evaluated the adversarial patches using the INRIA person dataset [11], which consists of 614 training images and 288 test images. To meet the input requirements of the detector, we padded all images with gray pixels to make them square and then resized them to 640×640 . Direct resizing would distort the image proportions. Furthermore, we evaluated the transferability of different adversarial patch methods on the MPII Human Pose dataset [1], COCO dataset [31] and 1,000 images from diverse scenarios collected from the Internet.

Attacked Models Our experiments attack a variety of detectors, including YOLOv3, YOLOv3-tiny [37], YOLOv4, YOLOv4-tiny [4], YOLOv5s [25], YOLOv7-tiny [44], FasterRCNN [38] and DETR [6]. We will abbreviate YOLO as YL and FasterRCNN as FRCNN for ease of presentation, such as YOLOv4-tiny as YLv4t. All models are

Table 1. Comparison of DiffPatch with other methods. Each metric contains two values: (AP% ↓ | ASR% ↑). Lower APs and higher ASRs indicate better attacks. The best results are **underlined**, and the top two results are in **bold**. † trained on YLv2, * trained on YLv4t.

Method	YLv3		YLv3t		YLv4		YLv4t		YLv5s		YLv7t		FRCNN		DETR	
	AP	ASR	AP	ASR	AP	ASR	AP	ASR	AP	ASR	AP	ASR	AP	ASR	AP	ASR
(P_A) AdvYL†	31.9	46.3	13.6	66.4	46.3	36.2	9.0	69.0	24.8	53.4	61.8	20.7	38.3	24.0	33.1	36.7
(P_B) T-SEA*	22.0	39.0	7.9	59.0	18.4	48.7	12.2	56.8	10.2	49.3	46.3	26.6	20.0	27.1	21.8	36.3
(P_C) NPAP*	50.4	33.7	15.9	74.2	61.3	26.2	13.7	78.9	41.0	41.4	69.0	17.5	55.5	25.1	43.3	41.5
(P_D) D2D*	50.3	33.9	18.8	69.1	58.4	30.9	15.6	75.0	41.0	40.7	68.7	18.4	52.9	25.0	44.8	34.2
(P_1) YL3(Ours)	12.9	70.4	17.0	64.1	58.2	28.1	21.3	60.4	36.0	52.2	60.2	24.6	38.6	29.3	38.6	38.6
(P_2) YL3t(Ours)	40.2	38.6	3.9	86.1	62.5	24.4	16.9	65.3	40.6	44.8	59.4	24.1	44.1	29.5	40.4	39.6
(P_3) YL4(Ours)	32.3	45.0	23.8	57.5	35.1	49.9	31.1	46.8	45.1	43.5	62.4	21.6	43.7	27.4	39.0	39.0
(P_4) YL4t(Ours)	40.8	41.0	11.8	73.6	61.6	25.5	9.2	79.1	38.3	50.3	57.4	25.7	45.3	28.4	39.5	41.4
(P_5) YL5s(Ours)	33.9	47.4	17.8	64.3	60.3	27.2	23.7	56.5	22.0	69.9	61.3	23.1	40.6	29.9	37.2	38.3
(P_6) YL7t(Ours)	49.6	35.0	19.9	64.3	64.2	23.0	26.0	56.7	39.6	44.5	51.7	33.5	50.2	26.1	42.2	38.9
(P_7) FRCNN(Ours)	38.8	42.7	19.9	62.4	58.1	29.2	23.0	60.8	37.2	50.7	61.7	24.3	22.6	38.5	35.4	43.7
(P_8) DETR(Ours)	46.6	35.2	35.2	49.0	67.1	22.1	34.3	46.7	44.6	43.1	66.8	20.5	46.2	26.1	37.1	42.0
(P_j) Source	53.5	29.7	45.9	38.1	70.0	18.5	47.8	36.9	55.8	35.0	69.4	18.4	53.5	23.3	47.3	33.6
Gray	72.3	16.5	61.8	25.2	76.8	12.8	56.4	30.0	74.1	15.5	77.1	13.5	64.4	17.3	50.2	34.4
(P_m) Random	70.2	16.9	64.3	22.2	78.5	12.2	60.4	26.9	75.1	15.5	79.8	12.3	67.3	17.6	51.1	31.7
(P_n) Random'	72.8	17.0	68.0	19.0	82.4	10.4	69.8	20.7	83.2	11.7	79.3	12.4	72.0	16.4	57.0	25.9

pre-trained on COCO dataset [31].

Implementation Details We treat person as the target attack class, set the batch size to 32, the maximum epoch $N_{iter} = 200$, DDIM sampling steps $T = 50$, unconditional embedding optimization iterations $N_u = 10$, $\eta_u = 0.01$, $\eta_p = 0.003$, $\epsilon = 0.5$, we use Adam optimizer [26] with the default parameters, the textual prompts \mathcal{P} are automatically generated using BLIP [29], the version of Stable Diffusion [39] is v1.4. Since we are generating irregular patches, we set the patch size to match the pixel area of a square patch with a scale of $\tau = 0.2$. To achieve stronger performance in patch attacks, we applied two iterations of optimization to the patch using DiffPatch. We regard the prediction of detector on clean data as the ground truth, and measure the capability of adversarial patch attack using the Average Precision (AP). A lower AP indicates that the accuracy of the detector in recognizing persons is reduced, indirectly indicating stronger patch attack performance. Additionally, since AP only measures the overall decline trend caused by the patches and does not directly reflect the attack performance, we also evaluated the Attack Success Rate (ASR) of various patches. The confidence threshold and IoU threshold for the detector are both set to 0.5. All of our experiments were conducted on a single NVIDIA Tesla A100.

4.2. Attack Performance Evaluation

We generated a series of adversarial patches targeting different models using DiffPatch and compared them with current patch generation methods on INRIA dataset, including AdvYL [43], T-SEA [22], NPAP [21], and D2D [30]. The detailed results can be seen in Table 1. DiffPatch ($P_1 - P_8$) performs comparably to the best existing non-natural patch generation methods in terms of the AP metric. Notably, DiffPatch achieved the best Attack Success Rate (ASR), with an improvement of **10.1%** over AdvYL on YLv4t. Compared to naturalistic adversarial patches (P_C and P_D), our patch trained on YLv4t effectively reduced the AP by **4.5%** and **6.4%**, and increased the ASR by **0.2%** and **4.1%**.

4.3. Cross-dataset Evaluation

Considering the relatively simple scenes in the INRIA dataset, we conducted tests to evaluate the attack performance of the patches in more diverse environments. We trained patches using YLv4t with various methods and tested them on multiple datasets, including MPII and COCO. Due to the large size of these datasets, we randomly sampled a subset of images containing people for testing, selecting 729 images from COCO and 569 images from MPII. Additionally, since the images from these two datasets are relatively outdated with low-resolution im-

ages, we also collected 1,000 high-resolution images from the Internet, representing diverse scenes (denoted as ‘‘Collected’’). The results, as shown in Table 2, demonstrate that our method significantly reduces the AP while substantially increasing the ASR. On average, the ASR shows a **17.5%** improvement over the unnatural patch method T-SEA and a **2.6%** improvement over the natural patch method NPAP.

Metric	Dataset	Attack			
		T-SEA	NPAP	D2D	Ours
AP%↓	INRIA	12.2	13.7	15.6	9.2
	MPII	17.0	17.3	17.9	12.5
	COCO	21.4	25.1	26.8	16.9
	Collected	8	6.7	7.2	3.9
ASR%↑	INRIA	56.8	78.9	75.0	79.1
	MPII	60.3	73.4	73.3	75.9
	COCO	54.5	63.9	60.3	67.8
	Collected	67.2	82.1	79.4	85.8

Table 2. Attack performance of different attacks across various datasets.

4.4. Ensemble Attack Evaluation

We employed an ensemble approach, training our patch using the averaged gradients from multiple models. Compared to other natural patch generation methods, our single patch achieved strong attack performance across various object detection models. As shown in Table 3, NPAP was trained on YL_v3 and YL_v4t, while D2D and our Diff-Patch were trained on all models. In white-box attacks, our method demonstrated a significant performance improvement over D2D.

4.5. Ablation Studies

Loss Function We conducted experiments using both the Common Detection Loss and IoU-Detection Loss under the same patch training setting. As shown in Figure 4, compared to the Common Detection Loss, our IoU-Detection Loss demonstrates greater stability during training process and achieves higher attack performance in a earlier time.

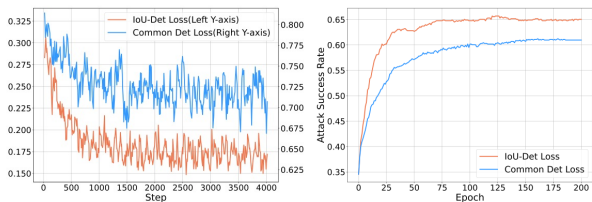


Figure 4. Comparison of two loss functions. *Left*: training loss; *Right*: attack performance.

Shape Impact The impact of patch shapes was investigated, as indicated by the data for P_m and P_n in Table 1. We compared the performance of random noise images with square and irregular shapes (with the same size as Diff-Patch). From the AP and ASR metrics, it is evident that square patches yield higher attack benefits compared to irregular patches. In other words, designing irregular patches with high attack success rates is more challenging.

Diffusion Trajectory Length Using latent vectors from intermediate timestamps to generate patches effectively mitigates semantic loss. We tested the results of latent vectors at different timestamps, evaluating the attack performance and similarity to textual descriptions for patches generated from diffusion trajectories of varying lengths. See Figure 5 for details. We use the cosine similarity of CLIP [35] embeddings to measure the alignment between the patch and the prompt, which indirectly reflects the visual quality of the patch. It is evident that starting diffusion optimization from $\frac{T}{2}$ (25 Steps) not only achieves a high success rate but also produces images that better align with textual descriptions, thereby maintaining greater semantic consistency with the original images.

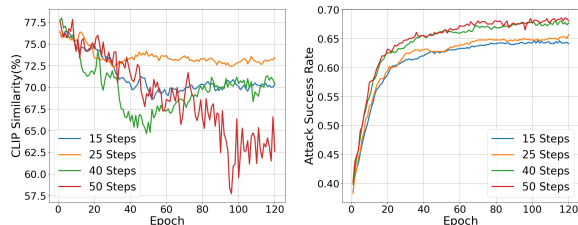


Figure 5. The effects of diffusion trajectories with different lengths on the performance of patch attacks and natural appearance.

Target Mask The target mask mechanism helps mitigate semantic loss in images to some extent. We compared the training results with and without the use of this mechanism. Without using target mask leads to quality issues in the patches during optimization, as shown in Figure 6.

Optimization Constraint We use the infinity norm to constrain each optimization of the patch to ensure its natural appearance. The size of ϵ significantly impacts patch generation. An appropriate ϵ can effectively balance the trade-off between attack performance and appearance. As shown in Table 4, we ultimately chose $\epsilon = 0.5$ as the constraint parameter for patch generation, as it maintains both appearance and a high attack success rate.

Iterative Optimization As the results in Table 5, iterative optimization can further enhance the adversarial strength of

Table 3. Attack performance of ensemble attacks of natural patch generation methods. Each metric contains two values: (AP% ↓ | ASR% ↑). White-box attacks are underlined, and the best results are in **bold**. Avg. refers to the average performance of white box attack.

Method	YLv3	YLv3t	YLv4	YLv4t	YLv5s	YLv7t	FRCNN	Avg.
	AP ASR	AP ASR	AP ASR	AP ASR	AP ASR	AP ASR	AP ASR	AP ASR
NPAP	<u>45.2</u> <u>34.2</u>	16.2 74.8	65.8 22.6	<u>19.3</u> <u>71.7</u>	57.4 28.5	70.8 17.3	57.8 24.0	<u>32.3</u> <u>53.0</u>
D2D	<u>48.9</u> <u>35.7</u>	<u>17.5</u> <u>66.8</u>	<u>58.4</u> <u>28.9</u>	<u>24.6</u> <u>59.3</u>	<u>35.6</u> <u>43.2</u>	<u>67.0</u> <u>19.5</u>	<u>52.7</u> <u>24.3</u>	<u>43.5</u> <u>39.7</u>
DiffPatch	<u>9.1</u> <u>65.9</u>	<u>6.1</u> <u>79.5</u>	<u>28.9</u> <u>47.4</u>	<u>12.0</u> <u>75.5</u>	<u>23.2</u> <u>62.4</u>	<u>55.4</u> <u>28.5</u>	<u>19.9</u> <u>38.9</u>	<u>22.1</u> <u>56.9</u>

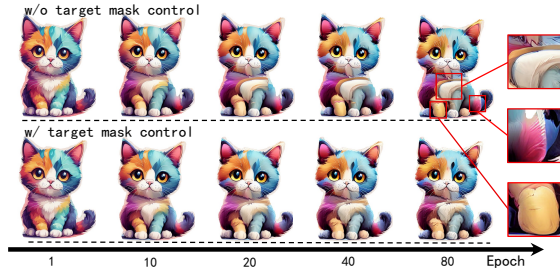


Figure 6. The impact of target mask on adversarial patch optimization. Without target mask control, adversarial patches exhibit noticeable detail distortions (indicated by red boxes).

Constraint ϵ	0.3	0.5	0.7
CLIP Sim.	75.6%	73.2%	63.9%
ASR	57.0%	63.0%	67.4%

Table 4. The effect of optimization constraint ϵ on latent vectors.

the patch. However, it also makes the patch unnatural.

Metric	Iterative	Model			
		YLv3t	YLv4t	YLv5s	FRCNN
AP%↓	w/o	7.1	12.3	24.6	26.0
	w/	3.9	9.2	22.0	22.6
ASR%↑	w/o	82.9	75.5	65.6	37.3
	w/	86.1	79.1	69.9	38.5
Sim.%↑	w/o	77.1	77.6	73.2	72.9
	w/	72.1	69.4	60.0	60.8

Table 5. The impact of using iterative optimization.

4.6. Physical-world Adversarial Patch Dataset

Our DiffPatch achieves promising attack results even in physical-world environments. Using DiffPatch, we designed 9 adversarial patches and printed them on T-shirts, as shown in Figure 7. We recruited 20 participants (with ethics approval) to capture images in diverse indoor and outdoor,

including laboratories, campus, cafeteria, subway station, and shopping mall. In total, we collected 1,131 images into our **AdvPatch-1K** dataset, including both individual and group (2 to 10+ persons) photos. The dataset is accompanied with detailed annotations of the person and patch locations (bounding boxes). Several example images are shown in Figure 1, with detailed statistics in Figure 8. The images in **AdvPatch-1K** can effectively evade the YOLOv5s detector, as shown in the right subfigure of Figure 8. Our dataset provides a valuable resource for advancing defense research against adversarial patch attacks. It is publicly available at <https://github.com/Wwangb/AdvPatch-1K>.



Figure 7. Adversarial T-shirts created using DiffPatch.

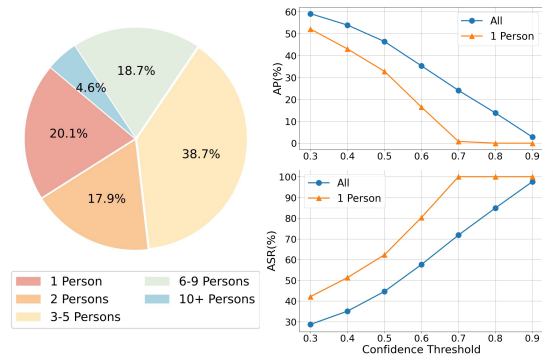


Figure 8. *Left*: The proportion of images with different numbers of persons in AdvPatch-1K. *Right*: The detection performance of YOLOv5s on AdvPatch-1K under different confidence thresholds.

5. Conclusion

In this work, we proposed a novel diffusion-based adversarial patch generation method *DiffPatch* to generate naturalistic and customized patches based on a reference image. DiffPatch utilizes image-to-latent mapping, incomplete diffusion optimization, and target mask control to create stylized adversarial patches. Extensive experiments across multiple object detection mod-

els validate the effectiveness of DiffPatch. With DiffPatch, we also created a physical-world adversarial dataset, *AdvPatch-1K*, comprising 1,131 images captured in diverse scenes and conditions. *AdvPatch-1K* can help develop robust defense methods against adversarial patch attacks.

References

- [1] Mykhaylo Andriluka, Leonid Pishchulin, Peter Gehler, and Bernt Schiele. 2d human pose estimation: New benchmark and state of the art analysis. In *CVPR*, pages 3686–3693, 2014. 5
- [2] Anish Athalye, Logan Engstrom, Andrew Ilyas, and Kevin Kwok. Synthesizing robust adversarial examples. In *ICML*, pages 284–293. PMLR, 2018. 2
- [3] Omri Avrahami, Dani Lischinski, and Ohad Fried. Blended diffusion for text-driven editing of natural images. In *CVPR*, pages 18208–18218, 2022. 3
- [4] Alexey Bochkovskiy, Chien-Yao Wang, and Hong-Yuan Mark Liao. Yolov4: Optimal speed and accuracy of object detection. *arXiv preprint arXiv:2004.10934*, 2020. 5
- [5] Tom B Brown, Dandelion Mané, Aurko Roy, Martín Abadi, and Justin Gilmer. Adversarial patch. *arXiv preprint arXiv:1712.09665*, 2017. 2
- [6] Nicolas Carion, Francisco Massa, Gabriel Synnaeve, Nicolas Usunier, Alexander Kirillov, and Sergey Zagoruyko. End-to-end object detection with transformers. In *ECCV*, pages 213–229. Springer, 2020. 5
- [7] Nicholas Carlini and David Wagner. Towards evaluating the robustness of neural networks. In *2017 IEEE Symposium on Security and Privacy (SP)*, pages 39–57. Ieee, 2017. 1
- [8] Chenyi Chen, Ari Seff, Alain Kornhauser, and Jianxiong Xiao. Deepdriving: Learning affordance for direct perception in autonomous driving. In *ICCV*, pages 2722–2730, 2015. 1
- [9] Xianyi Chen, Fazhan Liu, Dong Jiang, and Kai Yan. Natural adversarial patch generation method based on latent diffusion model. *arXiv preprint arXiv:2312.16401*, 2023. 2
- [10] Zhaoyu Chen, Bo Li, Shuang Wu, Kaixun Jiang, Shouhong Ding, and Wenqiang Zhang. Content-based unrestricted adversarial attack. *NeurIPS*, 36, 2024. 3, 5
- [11] Navneet Dalal and Bill Triggs. Histograms of oriented gradients for human detection. In *CVPR*, pages 886–893. Ieee, 2005. 5
- [12] Prafulla Dhariwal and Alexander Nichol. Diffusion models beat gans on image synthesis. *NeurIPS*, 34:8780–8794, 2021. 2
- [13] Bao Gia Doan, Minhui Xue, Shiqing Ma, Ehsan Abbasnejad, and Damith C Ranasinghe. Tnt attacks! universal naturalistic adversarial patches against deep neural network systems. *IEEE TIFS*, 17:3816–3830, 2022. 2
- [14] Ivan Evtimov, Kevin Eykholt, Earlene Fernandes, Tadayoshi Kohno, Bo Li, Atul Prakash, Amir Rahmati, and Dawn Song. Robust physical-world attacks on machine learning models. *arXiv preprint arXiv:1707.08945*, 2(3):4, 2017. 1
- [15] Kevin Eykholt, Ivan Evtimov, Earlene Fernandes, Bo Li, Amir Rahmati, Chaowei Xiao, Atul Prakash, Tadayoshi Kohno, and Dawn Song. Robust physical-world attacks on deep learning visual classification. In *CVPR*, pages 1625–1634, 2018. 1
- [16] Ian Goodfellow, Jean Pouget-Abadie, Mehdi Mirza, Bing Xu, David Warde-Farley, Sherjil Ozair, Aaron Courville, and Yoshua Bengio. Generative adversarial nets. *NeurIPS*, 27, 2014. 2
- [17] Ian J Goodfellow, Jonathon Shlens, and Christian Szegedy. Explaining and harnessing adversarial examples. *arXiv preprint arXiv:1412.6572*, 2014. 1
- [18] Amir Hertz, Ron Mokady, Jay Tenenbaum, Kfir Aberman, Yael Pritch, and Daniel Cohen-Or. Prompt-to-prompt image editing with cross attention control. *arXiv preprint arXiv:2208.01626*, 2022. 2
- [19] Jonathan Ho and Tim Salimans. Classifier-free diffusion guidance. *arXiv preprint arXiv:2207.12598*, 2022. 3
- [20] Jonathan Ho, Ajay Jain, and Pieter Abbeel. Denoising diffusion probabilistic models. *NeurIPS*, 33:6840–6851, 2020. 2
- [21] Yu-Chih-Tuan Hu, Bo-Han Kung, Daniel Stanley Tan, Jun-Cheng Chen, Kai-Lung Hua, and Wen-Huang Cheng. Naturalistic physical adversarial patch for object detectors. In *CVPR*, pages 7848–7857, 2021. 2, 6
- [22] Hao Huang, Ziyang Chen, Huanran Chen, Yongtao Wang, and Kevin Zhang. T-sea: Transfer-based self-ensemble attack on object detection. In *CVPR*, pages 20514–20523, 2023. 2, 6
- [23] Lifeng Huang, Chengying Gao, Yuyin Zhou, Cihang Xie, Alan L Yuille, Changqing Zou, and Ning Liu. Universal physical camouflage attacks on object detectors. In *CVPR*, pages 720–729, 2020. 1, 2
- [24] Steve TK Jan, Joseph Messou, Yen-Chen Lin, Jia-Bin Huang, and Gang Wang. Connecting the digital and physical world: Improving the robustness of adversarial attacks. In *AAAI*, pages 962–969, 2019. 2
- [25] Glenn Jocher, Alex Stoken, Jirka Borovec, NanoCode012, ChristopherSTAN, Liu Changyu, Laughing, tkianai, Adam Hogan, lorenzomamma, yxNONG, AlexWang1900, Laurentiu Diaconu, Marc, wanghaoyang0106, ml5ah, Doug, Francisco Ingham, Frederik, Guilhen, Hatovix, Jake Poznanski, Jiacong Fang, Lijun Yu, changyu98, Mingyu Wang, Naman Gupta, Osama Akhtar, PetrDvoracek, and Prashant Rai. *ultralytics/yolov5*, 2020. 5
- [26] Diederik P Kingma and Jimmy Ba. Adam: A method for stochastic optimization. *arXiv preprint arXiv:1412.6980*, 2014. 6
- [27] Alexey Kurakin, Ian J Goodfellow, and Samy Bengio. Adversarial examples in the physical world. In *Artificial intelligence safety and security*, pages 99–112. Chapman and Hall/CRC, 2018. 1, 2
- [28] Raz Lapid and Moshe Sipper. Patch of invisibility: Naturalistic black-box adversarial attacks on object detectors. *arXiv preprint arXiv:2303.04238*, 2023. 2
- [29] Junnan Li, Dongxu Li, Caiming Xiong, and Steven Hoi. BliP: Bootstrapping language-image pre-training for unified vision-language understanding and generation. In *ICML*, pages 12888–12900. PMLR, 2022. 6

- [30] Shuo-Yen Lin, Ernie Chu, Che-Hsien Lin, Jun-Cheng Chen, and Jia-Ching Wang. Diffusion to confusion: Naturalistic adversarial patch generation based on diffusion model for object detector. *arXiv preprint arXiv:2307.08076*, 2023. 2, 6
- [31] Tsung-Yi Lin, Michael Maire, Serge Belongie, James Hays, Pietro Perona, Deva Ramanan, Piotr Dollár, and C Lawrence Zitnick. Microsoft coco: Common objects in context. In *ECCV*, pages 740–755. Springer, 2014. 5, 6
- [32] Jiang Liu, Alexander Levine, Chun Pong Lau, Rama Chellappa, and Soheil Feizi. Segment and complete: Defending object detectors against adversarial patch attacks with robust patch detection. In *CVPR*, pages 14973–14982, 2022. 1
- [33] Riccardo Miotto, Fei Wang, Shuang Wang, Xiaoqian Jiang, and Joel T Dudley. Deep learning for healthcare: review, opportunities and challenges. *Briefings in bioinformatics*, 19(6):1236–1246, 2018. 1
- [34] Ron Mokady, Amir Hertz, Kfir Aberman, Yael Pritch, and Daniel Cohen-Or. Null-text inversion for editing real images using guided diffusion models. In *CVPR*, pages 6038–6047, 2023. 2, 3
- [35] Alec Radford, Jong Wook Kim, Chris Hallacy, Aditya Ramesh, Gabriel Goh, Sandhini Agarwal, Girish Sastry, Amanda Askell, Pamela Mishkin, Jack Clark, et al. Learning transferable visual models from natural language supervision. In *ICML*, pages 8748–8763. PMLR, 2021. 7
- [36] Aditya Ramesh, Prafulla Dhariwal, Alex Nichol, Casey Chu, and Mark Chen. Hierarchical text-conditional image generation with clip latents. *arXiv preprint arXiv:2204.06125*, 1(2):3, 2022. 2
- [37] Joseph Redmon and Ali Farhadi. Yolov3: An incremental improvement. *arXiv preprint arXiv:1804.02767*, 2018. 5
- [38] Shaoqing Ren, Kaiming He, Ross Girshick, and Jian Sun. Faster r-cnn: Towards real-time object detection with region proposal networks. *NeurIPS*, 28, 2015. 5
- [39] Robin Rombach, Andreas Blattmann, Dominik Lorenz, Patrick Esser, and Björn Ommer. High-resolution image synthesis with latent diffusion models. In *CVPR*, pages 10684–10695, 2022. 2, 5, 6
- [40] Chitwan Saharia, William Chan, Saurabh Saxena, Lala Li, Jay Whang, Emily L Denton, Kamyar Ghasemipour, Raphael Gontijo Lopes, Burcu Karagol Ayan, Tim Salimans, et al. Photorealistic text-to-image diffusion models with deep language understanding. *NeurIPS*, 35:36479–36494, 2022. 2
- [41] Mahmood Sharif, Sruti Bhagavatula, Lujo Bauer, and Michael K Reiter. Accessorize to a crime: Real and stealthy attacks on state-of-the-art face recognition. In *ACM CCS*, pages 1528–1540, 2016. 2
- [42] Jiaming Song, Chenlin Meng, and Stefano Ermon. Denoising diffusion implicit models. *arXiv preprint arXiv:2010.02502*, 2020. 3
- [43] Simen Thys, Wiebe Van Ranst, and Toon Goedemé. Fooling automated surveillance cameras: adversarial patches to attack person detection. In *CVPRW*, pages 0–0, 2019. 1, 2, 4, 6
- [44] Chien-Yao Wang, Alexey Bochkovskiy, and Hong-Yuan Mark Liao. Yolov7: Trainable bag-of-freebies sets new state-of-the-art for real-time object detectors. In *CVPR*, pages 7464–7475, 2023. 5
- [45] Xingxing Wei, Siyuan Liang, Ning Chen, and Xiaochun Cao. Transferable adversarial attacks for image and video object detection. *arXiv preprint arXiv:1811.12641*, 2018. 1
- [46] Zuxuan Wu, Ser-Nam Lim, Larry S Davis, and Tom Goldstein. Making an invisibility cloak: Real world adversarial attacks on object detectors. In *ECCV*, pages 1–17. Springer, 2020. 1, 2
- [47] Cihang Xie, Jianyu Wang, Zhishuai Zhang, Yuyin Zhou, Lingxi Xie, and Alan Yuille. Adversarial examples for semantic segmentation and object detection. In *ICCV*, pages 1369–1378, 2017. 1
- [48] Kaidi Xu, Gaoyuan Zhang, Sijia Liu, Quanfu Fan, Mengshu Sun, Hongge Chen, Pin-Yu Chen, Yanzhi Wang, and Xue Lin. Adversarial t-shirt! evading person detectors in a physical world. In *ECCV*, pages 665–681. Springer, 2020. 1, 2
- [49] Haotian Xue, Alexandre Araujo, Bin Hu, and Yongxin Chen. Diffusion-based adversarial sample generation for improved stealthiness and controllability. *NeurIPS*, 36, 2024. 2, 3
- [50] Yiqi Zhong, Xianming Liu, Deming Zhai, Junjun Jiang, and Xiangyang Ji. Shadows can be dangerous: Stealthy and effective physical-world adversarial attack by natural phenomenon. In *CVPR*, pages 15345–15354, 2022. 2
- [51] Xiaopei Zhu, Xiao Li, Jianmin Li, Zheyao Wang, and Xiaolin Hu. Fooling thermal infrared pedestrian detectors in real world using small bulbs. In *AAAI*, pages 3616–3624, 2021. 2
- [52] Xiaopei Zhu, Zhanhao Hu, Siyuan Huang, Jianmin Li, and Xiaolin Hu. Infrared invisible clothing: Hiding from infrared detectors at multiple angles in real world. In *CVPR*, pages 13317–13326, 2022. 2